Stimulated Raman scattering from symmetrically illuminated two-layered spherical targets with 527 nm laser light

M. Tsukamoto, K. A. Tanaka,[a] K. Mima, M. Kado, S. Miyamoto, M. Nakai, T. Norimatsu, M. Takagi, K. Nishihara, T. Yamanaka, and S. Nakai
Institute of Laser Engineering, Osaka University, Yamada-oka 2-6, Suita, Osaka 565, Japan

A. Nishiguchi
Osaka Institute of Technology, Asahiku, Osaka 535 Japan

(Received 28 June 1994; accepted 14 October 1994)

Spectrally shifted Raman light with time was observed from two-layered spherical targets irradiated with 527 nm random phased laser light. The target was composed of a foam shell and an outer thin plastic layer. The Raman spectrum shifted rapidly to the short-wavelength side during the laser pulse. The start timing was earlier than that of the usually observed Raman light at an experiment with a single-layered plastic shell target. It was inferred that a plasma shoulder with a long scale length moved outward on the expanding plasma, consistent with the observed Raman light. © *1995 American Institute of Physics.*

I. INTRODUCTION

Stimulated Raman scattering (SRS) is one of parametric instabilities in which an incident electromagnetic light wave decays into a scattered-light wave and an electron–plasma wave.[1] The frequencies and wave vectors of these three waves have the relations of $\omega_0=\omega_s+\omega_{\mathrm{EPW}}$ and $\mathbf{k}_0=\mathbf{k}_s+\mathbf{k}_{\mathrm{EPW}}$, where ω_0, ω_s, and ω_{EPW} and $\mathbf{k}_0$, $\mathbf{k}_s$ and $\mathbf{k}_{\mathrm{EPW}}$ denote the frequencies and the wave vectors of the incident electromagnetic light, and scattered-light and electron–plasma waves. The dispersion relations of the three waves are

$$\omega_0^2=\omega_{pe}^2+c^2\mathbf{k}_0^2, \tag{1}$$

$$\omega_s^2=\omega_{pe}^2+c^2\mathbf{k}_s^2, \tag{2}$$

$$\omega_{\mathrm{EPW}}^2=\omega_{pe}^2+3\,\nu_{\mathrm{th}}^2\mathbf{k}_{\mathrm{EPW}}^2. \tag{3}$$

Here ω_{pe} is electron plasma frequency, c is the speed of light, and ν_{th} is the electron thermal velocity, $(T_e/m_e)^{1/2}$, where m_e is the electron mass. The scattered-light wave could reduce the fusion efficiency by carrying the laser energy away from the target, and the electron–plasma wave could preheat the fuel[2] by hot electrons through the wave damping.[3–5] The SRS can be excited in the corona plasma of electron densities $n_e\leqslant 0.25n_{\mathrm{cr}}$, where n_{cr} is the critical density.[1] In order to achieve laser implosions with high efficiency, it is important to understand the detailed mechanisms of the SRS and to minimize or control the SRS in the laser-produced plasmas.

Several types of cryogenic targets have been proposed and developed for laser inertial confinement fusion (ICF).[6,7] One of the candidates to produce a high gain in ICF is a two-layered spherical (TLS) target, which is composed of liquid or solid deuterium tritium fuel layer sustained by a plastic foam shell coated with a plastic layer.[8] The TLS targets have been successfully introduced to implosion experiments.[9] A TLS target at the laser firing position was filled up with high-pressure deuterium fuel gas up to 11 MPa at room temperature, and was cooled down to a cryogenic temperature (~18 K) to form liquid or solid fuel in the inner foam layer before laser irradiation.[8] The TLS target with 4 μm outer plastic thickness has been chosen to fill up TLS targets with deuterium fuel in the implosion experiment. We observed special Raman light occasionally with the TLS target with the fuel. The Raman light starts at a later time during the laser pulse, since it takes enough time to ablate the 4 μm outer plastic layer. This Raman light is to be shown later as the spectrally shifted Raman light with time, and is considered to relate with the inner foam ablation. In order to measure the Raman light reproducibly before the laser peak, the TLS targets with 1 μm plastic layer were mainly used to burn through it earlier. The TLS targets with the 1 μm plastic layer were not filled up with deuterium fuel, since the plastic layer could not hold the high deuterium pressure.

The intense SRS was observed when the laser light irradiates a simple foam shell target without fuel and any outer plastic layer,[10] but was rather different from the one above. The SRS was strongly modulated in both time and spectrum. However, for a foam shell filled up with deuterium fuel, only the weak SRS was observed. The SRS from the foam shell without fuel was four to five times stronger than the SRS from the foam shell saturated with fuel. It was interpreted that the strong filamentation or self-focusing could be responsible, since the laser light could experience the strong density perturbation of the porous structures, such as plastic foam without fuel.[10] When the laser directly interacts with the inner foam layer without fuel after ablating the outer thin plastic layer of the TLS target, the SRS could be strongly excited in the corona, in addition to the spectrally shifted Raman light with time.

In this paper, we report temporally and spectrally resolved measurements of the SRS mainly from two-layered spherical targets. The Raman light reported here was rather different from the normally observed one with single-layered targets such as a plastic shell and a foam shell with or with-

[a]Also at the Department of Electromagnetic Energy Engineering, Osaka University, Yamada-oka 2-1, Suita, Osaka 565 Japan.

 1070-664X/95/2(2)/486/7/$6.00

TABLE I. Experimental parameters of targets and incident laser TLS: Two-layered spherical target; PS: plastic shell target.

Experiment No.	Target type	Diameter (μm)	Thickness of plastic layer (μm)	Thickness of foam layer (μm)	Density of plastic layer (g/cm^3)	Density of foam layer (g/cm^3)	Number of beams	Intensity (10^{14} W/cm^2)	Pulse width (FWHM: ns)
1	TLS	500	1	52.2	1.38	0.2	12	4	1.7
2	TLS	545	1	13.6	1.38	0.5	12	3	1.7
3	TLS	635	1	17.7	1.38	0.5	12	3	1.7
4	TLS	635	1	44.3	1.38	0.2	3	3	1.7
5	PS	633	8.38	···	1.10	···	12	3	1.7
6	Thin plastic	···	1.13	···	1.10	···	1	1.2	2.2

out fuel. We inferred a plasma shoulder on the expanding plasma to explain the Raman light. The Raman light could be excited on the plasma shoulder with a long scale length. Then the spectral shift of the Raman light with time was due to a decrease of the plasma shoulder density. We estimate the spatial size of the plasma shoulder and indicate that the plasma shoulder goes out of the expanding plasma. In Sec. II the experimental conditions and setup are described. In Sec. III experimental results are shown. In Sec. IV we discuss the experimental results with the Raman light and its origin. Finally, we summarize in Sec. V.

II. EXPERIMENTAL CONDITIONS

Six types of experiments, as shown in Table I, were performed with 527 nm random phased laser light of the GEKKO XII 12 beam glass laser system[11] at the Institute of Laser Engineering, Osaka University. The 527 nm light was focused onto the spherical target by a $f/3$ lens with $d/R = -5$, where d and R are the defocusing distance and the target radius. The 527 nm light was obtained by frequency doubling of the Nd-doped glass laser light in potassium dihydrogen phosphate (KDP) crystals. Random phase plates (RPP) were inserted in front of each focus lens to create uniform irradiation spots.[12] For $d/R = -5$ and using RPPs, the spot size at the target position is almost the same as the target diameter. The unconverted 1053 nm beam was about 1 cm in diameter at the green focus, thus creating an about 10^{11} W/cm^2 intensity.

The configuration of GEKKO XII laser irradiation is shown in Fig. 1(b) together with a Cartesian coordinate system with x, y, and z axes. The spherical target was placed at the point of the diagonal intersection in the rectangles. Figure 1(a) shows that the axes of four laser beams on the same plane coincide with the diagonal lines in each rectangle. The arrows on the diagonal lines indicate the propagating directions of the four beams. One rectangle including four beams was perpendicular to other two rectangles, as shown in Fig. 1(b), resulting in the symmetric irradiation with the 12 beams. Our observation system viewed the target at a polar angle of 142.6° from $\mathbf{k}_0$ of the closest incident beams, which were No. 2, No. 7, and No. 8 beams in Fig. 1(b).

The light was collected by two concave aluminum mirrors and was guided to a 0.25 m grating spectrometer coupled to an optical streak camera (S-1 photo cathode) to measure the time-resolved SRS spectrum. The target was image relayed on the slit of the spectrometer. The field of view was determined by the incident-slit sizes of both spectrometer and the S-1 streak camera, and was about 200 (V)×600 (H) μm on the target. The spectral and temporal resolutions were 10 nm and 60 ps, respectively. The spectral range was from 700 to 1053 nm. Colored-glass filters were used to attenuate the scattered incident light (527 nm) and to block unwanted grating orders. Bandpass filters were also used to attenuate the scattered $\omega_0/2$ light (1053 nm). By these bandpass filters, the transmission of scattered light decreased sharply at above 1020 nm. The $3\omega_0/2$ emission (351 nm) was measured with another optical streak camera (S-20 photo

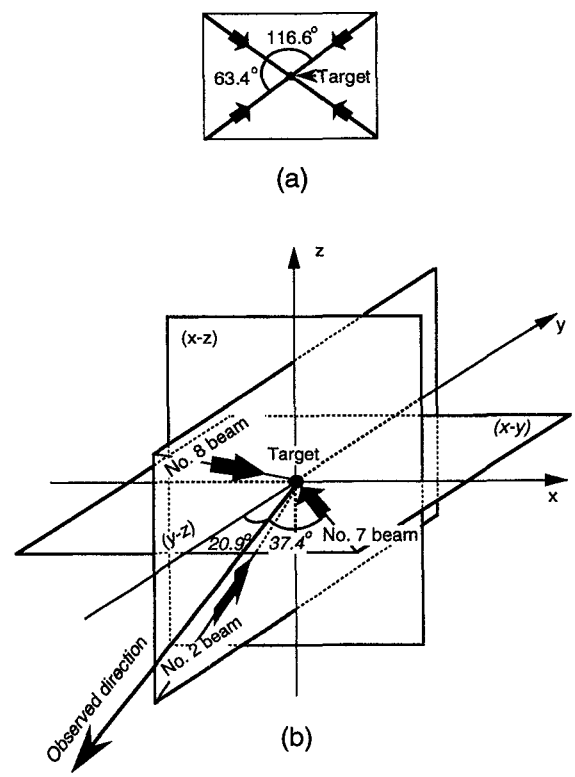

FIG. 1. Configuration of laser irradiation with GEKKO XII 12-beam glass laser system. (a) The axes of four beams on the same plane out of 12 beams coincide with the diagonal lines in each rectangle. The arrows on the diagonal lines indicate the propagating directions of the four beams, respectively. (b) One rectangle including the four beams was perpendicular to the other two rectangles, resulting in the symmetric irradiation with the 12 beams. Our observation system viewed the target at a polar angle of 142.6° from $\mathbf{k}_0$ of the closest incident beams (No. 2, No. 7, and No. 8 beams).

cathode), coupled with an optical fiber as an evidence of two-plasmon decay instability (TPD).[13] The TPD is also an instability that the electromagnetic wave decays into two plasma waves and takes place at a density $n_e \sim n_{cr}/4$. The optical system using the light collector was the same as the one for SRS. The collected light was split with a quartz plate and was guided to the collecting lens of an optical fiber through interference filters to choose the 351 nm light, whose spectral bandwidth was 6 nm (full width at half-maximum, FWHM). Time fiducials were introduced on the optical streak cameras, making use of a portion of the input laser light.

Experimental parameters of targets and incident laser are listed in Table I. Three different targets, namely, the two-layered spherical (TLS), the plastic shell (PS), and the thin foil plastic targets were used in experiments No. 1–6, respectively. Thickness of the outer-plastic layer of all TLS targets was 1 μm, and all TLS targets could not be filled up with fuel, as described in the Introduction. The difference in the target condition between experiments No. 1 and No. 2 was the inner foam density, namely 200 mg/cm^3 in experiment No. 1 and 500 mg/cm^3 in experiment No. 2. For experiment No. 3, the inner foam density was the same as the one in experiment No. 2. The diameters of the TLS targets used in experiments No. 2 and 3 were 545 and 635 μm, respectively. Two different diameters in experiments No. 2 and No. 3 were used to study the target diameter dependence on the Raman light. In experiment No. 4, the TLS target with a 635 μm diam was irradiated with No. 2, No. 7, and No. 8 beams near the observed direction shown in Fig. 1(b). The intensity of spatially overlapped regions with the three beams was 3×10^{14} W/cm^2. The PS and the thin foil plastic targets were used to compare the results using the TLS targets. Except experiments No. 4 and 6, 12 beams were used. In the case of 12 beam irradiations, the laser intensity was 4×10^{14} W/cm^2 in No. 1 and 3×10^{14} W/cm^2 in experiments No. 2, No. 3, No. 5, where these intensities were determined by the total incident laser energy divided by the target surface area and the pulse duration. The shape of the laser pulse was rectangular with the widths (FWHM) of 1.7–2.2 ns, and with the rise time (10%–90% of the peak intensity) of 600 ps.

III. EXPERIMENTAL RESULTS

Streak images of SRS spectra observed in experiments No. 1, 2, 3, 5, and 6 are shown in Figs. 2(a)–2(e). The horizontal and vertical axes represent the wavelength and time. The contours are equal intervals of relative intensity. We observed the spectrally shifted Raman light with time (SSRT) from TLS targets as shown in Figs. 2(a)–2(c). As shown in Fig. 2(a), the edge of the SSRT started at +400 ps, and shifted from 980 to 800 nm in 400 ps for the dry TLS target with a 1 μm outer-plastic layer. The peak spectral intensity is more than 70 times the background plasmas emission. The maximum spectral and the temporal widths (FWHM) through all the spectral shifts are about 30 nm and 110 ps, respectively. The SSRT in Fig. 2(b) was emitted in a wide spectral region, such as the one in Fig. 2(a). The edge of the SSRT spectra in Fig. 2(b) started at +400 ps and shifted from 980 to 800 nm in 400 ps. The peak spectral

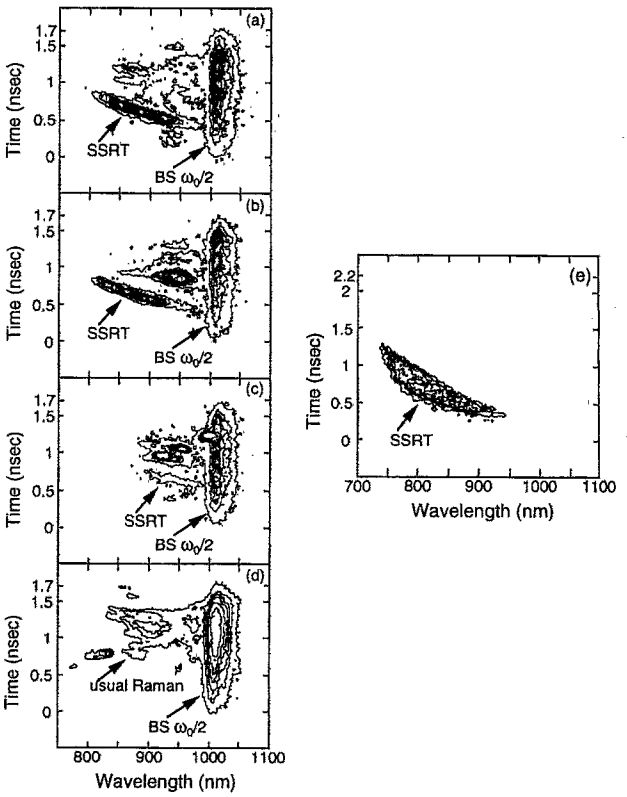

FIG. 2. Streak images of SRS spectra observed in the condition shown in Table I. (a), (b), (c), (d), and (e) correspond to experiments No. 1, 2, 3, 5, and 6, respectively. The spectrally shifted Raman light with time (SSRT) from TLS targets are observed in (a), (b), and (c). A similar result is observed with the thin foil plastic target, as shown in (e).

intensity is also 70 times stronger than the background. The maximum spectral and the temporal widths (FWHM) are about 25 nm and 100 ps, respectively. In Fig. 2(c), the SSRT started at +550 ps and shifted from 980 to 900 nm in 100 ps. The intensity of the SSRT spectra between 930 and 980 nm in Fig. 2(c) is almost the same as the one in Fig. 2(b). Between 900 and 930 nm, intensity of the SSRT in Fig. 2(c) is about one-third of the one in Fig. 2(b). In the spectral region below 900 nm, the intensity of the SSRT in Fig. 2(c) is less than the detection level. The difference with the SSRT between Figs. 2(b) and 2(c) is the target diameters, 545 μm for Fig. 2(b), and 635 μm for Fig. 2(c). In experiment No. 4 using three beams, the SSRT was not observed from the TLS target with 635 μm in diameter.

For the plastic shell (PS) target, we did not observe the SSRT, as shown in Fig. 2(d). In Fig. 2(d), the SRS from the imploding PS target was the usually observed one (usual Raman) at $I_L=3\times10^{14}$ W/cm^2, starting at +1 ns between 800 and 950 nm. The peak spectral intensity was only ten times more than the background plasma emission.

In experiments No. 1, 2, and 3, the SSRT were emitted at an early time (+400, +400, and +550 ps) during pulse duration. The usual Raman from the PS target was not observed at these times, but rather at a later time (+1 ns). This indicates that the hot electron preheating of the target via the

SSRT could be important, because of the early timing.

The other Raman components were also observed after the SSRT occurred, as shown in Figs. 2(a)–2(c). The features of the Raman components differ in each experiment. For the TLS target, the Raman component in Fig. 2(a) is temporally and spectrally modulated between 800 and 950 nm. The foam density of the TLS target in Fig. 2(a) was 0.2 g/cm^3, as indicated in Table I. For the foam density of 0.5 g/cm^3 in Fig. 2(b), the Raman component is strongly emitted between 900 and 980 nm and started at +800 ps. In Fig. 2(c) with a 0.5 g/cm^3 foam density, the strong Raman component is also shown between 900 and 980 nm and started at +850 ps. The density of the inner foam layer varied depending on the state of the porous. These observed features imply that the growth of the SRS could be related to the density nonuniformity in the foam, even after the plastic layer is ablated away.

The spectral feature shown in Fig. 2(e) could be obtained using a thin foil plastic target. One can see that this spectrum is a reproduction of the results by Villeneuve *et al.*[14] and Labaune *et al.*[15] The edge of the Raman light in Fig. 2(e) started at +290 ps and shifted from 930 to 740 nm in 960 ps. The maximum spectral and the temporal width (FWHM) are 55 nm and 340 ps, respectively. This spectral shift with time was also interpreted as the decay of the peak plasma density with time in this case.

At the spectral region between 1030 and 980 nm in Fig. 2(a), there is another major spectral component, the blue-shifted component of $\omega_0/2$ light (BS $\omega_0/2$ light), starting from 0 to 1.7 ns. The BS $\omega_0/2$ light has been observed all the time during laser pulse for every target shot, except the case of a thin foil target, as shown in Fig. 2(e). This spectrum is the same as the one reported previously by Turner *et al.*, who found the spectrum with double peaks, and called it "Raman-like scattering."[13] We note that the BS $\omega_0/2$ light was present as peaked spectra centered at 1020 nm due to the used bandpass filters. The short-wavelength cutoff of the BS $\omega_0/2$ light spectra was 980 nm. There should be the other component scattered at a longer wavelength than $\omega_0/2$, which was the red-shifted component of "Raman-like scattering."[13] This could not be observed, due to the greatly decreased sensitivity of our observation system with the bandpass filters. They inferred that both components of "Raman-like scattering" were induced by two plasma waves due to TPD, two-plasmon decay instability. During all the time when the BS $\omega_0/2$ light was scattered, we could observe the $3\omega_0/2$ light caused by the TPD. Those observations indicate that the scattering of the BS $\omega_0/2$ light and TPD were generated simultaneously.

The temporally modulated Raman light was emitted at about 980 nm between +800 and +1400 ps in Fig. 2(a). Such a signal was often observed at the implosion experiments using spherical targets, as shown in Figs. 2(c) and 2(d).

IV. DISCUSSION

The SSRT, spectrally shifted Raman light with time, was also reproduced in experiment No. 6 using a plastic thin foil target in Fig. 2(e). In the $3\omega_0/2$ measurement of experiment No. 6, the signal of $3\omega_0/2$ disappeared before the SSRT emitted. This indicates that the maximum density of the plasmas at the SSRT emission decreased to below $n_{cr}/4$. The SRS threshold on the top of expanding plasma is lower than the one on the surrounding plasma, because convective losses of scattered-light and electron–plasma waves due to the density gradient are weak on the flat density region with the scale length $L_p \sim \infty$, such as a top of a parabolic density profile. In the thin foil plastic target case, the SSRT is explained by the decrease of the maximum density of the parabolic profile with time. In order to understand the emission behavior of SSRT from the TLS target, as shown in Figs. 2(a)–2(c), we introduce a plasma shoulder with a scale length ($L_p \sim \infty$) larger than the one (L_a) of the surrounding plasma. The density of the plasma shoulder decreases as the shoulder expands with time. Since the effective SRS threshold on the shoulder becomes low, the SSRT can be expected to occur on the shoulder. The introduction of the plasma shoulder is supported by a theoretical prediction[16] that the SRS can be actually excited on the plasma shoulder, and shifts to the shorter wavelength as the density of the plasma shoulder decreases.

For the 635 μm diam target, the SSRT shifted only to 900 nm, as shown in Fig. 2(c) though the SSRT shifted down to 800 nm for the targets with 545 μm in diameters, as shown in Fig. 2(b). The dampings of the scattered-light wave (SLW) and the electron–plasma wave (EPW) determine the threshold for the SSRT in a homogeneous plasma ($L_p \sim \infty$).[17,18] The threshold in a homogeneous plasma is given by[17,18]

$$\frac{\gamma_0^2}{\gamma_s \gamma_{\mathrm{EPW}}} > 1. \tag{4}$$

Here γ_0 is the SRS growth rate in a homogeneous plasma ($L_p \sim \infty$), and is given by

$$\gamma_0 = \frac{1}{4} k_{\mathrm{EPW}} \nu_{\mathrm{os}} \left(\frac{\omega_{pe}^2}{\omega_s \omega_{\mathrm{EPW}}} \right)^{1/2}, \tag{5}$$

where $\nu_{\mathrm{os}} = 25.6 \times 10^{-3} I_L^{0.5} \lambda_0$ is the oscillating velocity in the laser electric field. Here I_L and λ_0 are the intensity and wavelength of the incident laser in units of W/cm^2 and nm. In addition, γ_s and γ_{EPW} are the damping rates of the SLW and the EPW, respectively, where $\gamma_s = (\gamma_{ei}/2)(\omega_{pe}/\omega_s)^2$ and $\gamma_{\mathrm{EPW}} = \gamma_{ei}/2 + \gamma_{Ld}$, with γ_{ei} and γ_{Ld} being the electron–ion collision frequency and the Landau damping rate.[18] Here γ_{ei} is a function of the temperature T_e in keV, the electron density n_e in cm^{-3}, and the effective ion charge (Z), and γ_{Ld} is a function of T_e and n_e. At the time of the SSRT short-wavelength cutoff in these TLS target experiments T_e and Z are predicted with the one-dimensional (1-D) hydrodynamic code "HIMICO"[19,20] to be 3.5 and 1.8–2.0 keV for 545 and 635 μm targets. The laser intensity is the same for both targets, as shown in Table I. Therefore the values of γ_0, γ_s, and γ_{EPW} are the same and the difference with the short-wavelength cutoff of the SSRT cannot be explained with Eq. (4), between the 545 and 635 μm target experiments. From the evaluation of Eq. (4), where γ_0 is calculated with the intensity per beam as I_L ($=10^{14}$ W/cm^2), instead of the values shown in Table I, it is indicated that the SSRT can be

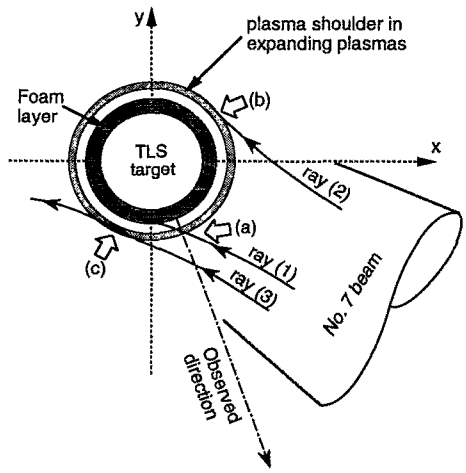

FIG. 3. Schematic configuration of the propagation of rays (1), (2), and (3) in the No. 7 beam to positions (a), (b), and (c) on the plasma shoulder on the expanding plasma.

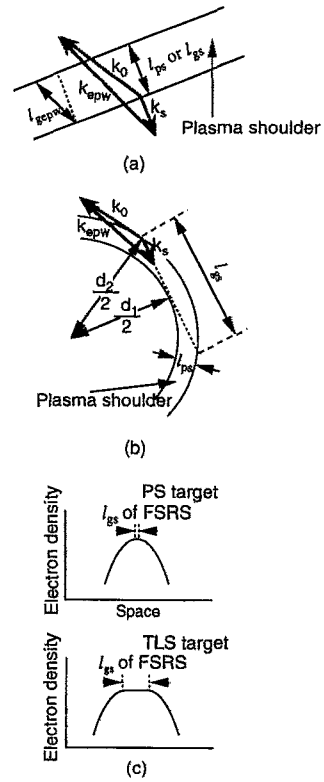

FIG. 4. (a) schematically shows position (a) in Fig. 3. The $\mathbf{k}_s$ in (b) shows the SLW of ray (2) shown at position (b) in Fig. 3. The parabolic density profiles experienced by ray (3) at position (c) in Fig. 3 for the PS and the TLS targets are shown in (c). The interaction length l_{gs} of forward SRS for the PS target is shorter than the one for the TLS target, since the plasma shoulder is not present on expanding plasma for the PS target.

caused in a homogeneous plasma because of $400>\gamma_0^2/(\gamma_s\gamma_{\mathrm{EPW}})>9$ in the spectral region between 750 and 1050 nm for 545 and 635 μm target experiments. This result cannot explain even that the short-wavelength cutoff of the SSRT was observed in the spectral region more than 800 nm. We interpret that the short-wavelength cutoff of the SSRT was limited by some other reasons instead of the dampings of the SLW and the EPW in a homogeneous plasma.

The Raman spectrum shifted with time observed here contains a spatial information, in addition. The field of view mainly covers the overlapped region of No. 2, No. 7, and No. 8 beams and the greater part of their near-backscattered light. Figure 3 shows schematically typical propagating rays (1), (2), and (3) in beam No. 7, the observed direction and the plasma shoulder on the expanding plasma from the TLS target. Here, we assume that the plasma shoulder could propagate to the outward direction from the TLS target, and that the position on the shoulder where the SSRT occurred could walk out of the field of view. The observation direction of the light emission coincides with the propagation direction of the plasma shoulder at the position (a). If the SSRT occurs at the position (a), the SSRT should be observed until 750 nm, at least as estimated with Eq. (4). In the experimental results, the SSRT is limited even at 800 and 900 nm for 545 and 635 μm targets, respectively. Thus, this inconsistency leads us to conclude the observed SSRT was not emitted at the position (a). In the three-beam experiment (No. 4 in Table I) with the No. 2, 7, and 8 beams, the SSRT was not observed, as described in Sec. III. We interpreted that the length of the plasma shoulder, l_{ps}, in the overlapped region of the beams was almost same as l_{ps} at the position (a) in Fig. 3 for the No. 3 12-beam experiment. The laser intensity on the overlapped region of the three beams was 3×10^{14} W/cm^2, the same as the intensity at position (a) in Fig. 3 for the 12-beam experiment. Position (a) existed in the region overlapped by mainly No. 2, 7, and 8 beams, even for the 12-beam experiment. Outside the overlapped region, l_{ps} may not be produced, since the intensity there was two or three times lower than the overlapped irradiation intensity. The SSRT could not be caused, even in the overlapped region of three beams, where the condition with l_{ps} for the 12-beam experiment was kept. We interpret that the SSRT was not from point (a) in Fig. 3, which was in the overlapped region of the No. 2, 7, and 8 beams in the 12-beam experiment.

We estimate the length, l_{ps}, of the plasma shoulder with $L_p\sim\infty$ under the condition that the SSRT could not occur at position (a). If we include the convective losses, the propagation of the SLW and the EPW introduces effective damping rates, ν_{gs}/l_{gs} and $\nu_{g\mathrm{EPW}}/l_{g\mathrm{EPW}}$, where $\nu_{gs}=c[1-(\omega_{pe}/\omega_s)^2]^{1/2}$, $\nu_{g\mathrm{EPW}}=(\frac{3}{2})(k_{\mathrm{EPW}}/\omega_{\mathrm{EPW}})\nu_{\mathrm{th}}^2$, $l_{gs}=\alpha l_{\mathrm{ps}}$ and $l_{g\mathrm{EPW}}=\beta l_{\mathrm{ps}}$ are the group velocities of the SLW and the EPW, the interaction lengths of the SLW and the EPW, respectively. The α and the β are geometrical variable factors, which correlate the length of the plasma shoulder to the interaction length and are determined by the propagation position of the rays. Both factors are equal to or larger than 1, or namely l_{gs} and $l_{g\mathrm{EPW}}$ are equal to l_{ps} or longer than l_{ps}. These relations are shown in Figs. 4(a) and 4(b) at the positions that correspond to ones in Figs. 3(a) and 3(b). Inserting these damping rates into the equation of the threshold for SRS in a homogeneous plasma,[17,18] a threshold expression due to convective losses in a finite homogeneous plasma is

$$\frac{\gamma_0^2}{\nu_{gs}\nu_{g\mathrm{EPW}}}\alpha\beta l_{\mathrm{ps}}^2 > 1. \tag{6}$$

Now we focus on position (a), where the l_{ps} is probably not long enough to excite the SSRT. This condition is obtained by reversing the sign of inequality in Eq. (6), and then the l_{ps} could be estimated. Here l_{gs} is equal to l_{ps}, namely $\alpha=1$, since the direction of $\mathbf{k_s}$ is normal to the tangential line of the plasma shoulder, as shown in Fig. 4(a). We use the frequency and wave number matching conditions indicated in the Introduction, in addition to Eqs. (1)–(3) and (4) to calculate values of ν_{gs}, $\nu_{g\mathrm{EPW}}$, γ_0, and β. Here ν_{gs} is 1.53×10^{10} (cm/s) when the wavelength of the SLW, λ_S, is 980 nm. In addition, $\nu_{g\mathrm{EPW}}$, and γ_0 and β are dependent on the incident angle of the ray (1) to the plasma shoulder in addition to the electron temperature, T_e, of 2 keV. When the refraction of the ray (1) is neglected and the incident angle is 37.4°, $\nu_{g\mathrm{EPW}}$ and γ_0 and β are 4.20×10^8 (cm/s), 4.15×10^{12} (l/s) and 1.14, respectively. The length of the plasma shoulder, l_{ps}, is found to be less than 5.7 μm. When the refraction of the ray (1) is considered and the incident angle is 90°, maximum values, $\nu_{g\mathrm{EPW}}$, γ_0, and β are 3.51×10^8 (cm/s), 3.46×10^{12} (l/s), and 3.39. Then l_{ps} is found to be less than 3.6 μm.

The SLW of the ray (2) shown at position (b) in Fig. 3 propagates along the tangential line, as shown with $\mathbf{k_s}$ in Fig. 4(b). The interaction length l_{gs} of the SLW in Fig. 4(b) is longer than the one of the SLW in Fig. 4(a), and is given by

$$l_{gs}=2\left[\left(\frac{d_2}{2}\right)^2-\left(\frac{d_1}{2}\right)^2\right]^{1/2}, \tag{7}$$

where d_1 is larger than the target diameter when the plasma shoulder moves outward before the shell begins moving inward direction, and d_2 is (d_1+2l_{ps}). When d_1 is longer than the 635 μm (or 545 μm) target diameter and l_{ps} of the plasma shoulder is 5.7 or 3.6 μm, the l_{gs} becomes longer than 121 or 96 μm (or 112 or 89 μm). The relation of l_{gs} and l_{ps} are given by $l_{gs}>21l_{\mathrm{ps}}$ or $l_{gs}>27l_{\mathrm{ps}}$ (or $l_{gs}>20l_{\mathrm{ps}}$ or $l_{gs}>25l_{\mathrm{ps}}$). In each case, Eq. (6) is satisfied, even if we take the smallest β (=1). Thus, the SSRT could grow at position (b), while the SSRT is not excited at position (a).

There could be a possible mechanism that could excite the SSRT due to ray (3) at position (c) in Fig. 3 in our experimental condition. Villeneuve and Baldis proposed that a feedback loop formed in a parabolic density profile can drive an intense backward SLW with the absolute growth of SRS.[14,15] For the implosion experiment, the parabolic density profile is experienced by ray (3) in Fig. 3. In a feedback loop mechanism, the generation of the forward SRS (FSRS) is necessary on the top of the parabolic profile. The possible parabolic density profiles for the PS (plastic shell) and the TLS (two-layered spherical) targets are shown in Fig. 4(c). The l_{gs} of FSRS for the PS target is shorter than the one for the TLS target, as shown in Fig. 4(c), since the plasma shoulder is not present on the expanding plasma for the PS target. At the early time of the laser pulse, the SSRT and the other SRS signals, except for the BS $\omega_0/2$ light were not observed for the PS target, as shown in Fig. 2(d). For the PS target, we consider the convective losses might dominate the FSRS growth. For the TLS target, since the plasma shoulder exists, the convective losses could be overcome by the FSRS growth. Therefore, the backward SLW of ray (3) at position (c) could be caused due to a feedback loop mechanism in the parabolic density profile experienced by ray (3). However, our observed direction is not the same as the direction of the backward SLW of ray (3). If the SSRT is the backward SLW of ray (3), we might observe the refracted light of the backward SLW. In this case, the SSRT could be caused at position (c).

We indicate that the SSRT could be caused at positions (b) and (c) in Fig. 3, while it is not possibly excited at position (a) in Fig. 3. To explain that the SSRT from positions (b) and (c) walks out of the field of view, the plasma shoulder should propagate outward from the target, as assumed before. When the propagation velocity of plasma shoulder is the same between 635 and 545 μm target experiments, the region in which the SSRT occurs for a 635 μm target can walk out of the field of view faster than for the 545 μm target, since positions (b) and (c) for a 635 μm target are the outside of positions (b) and (c) for the 545 μm target in the field of view. Therefore, the SSRT for the 635 μm target shifted only to 900 nm, as shown in Fig. 2(c), though the SSRT for the 545 μm target shifted down to 800 nm, as shown in Fig. 2(b).

We consider if the ablation of the thin plastic layer and the direct laser irradiation on the foam layer could be related to the SSRT. The SSRT from the TLS targets started +400, +400, and +550 ps in Figs. 2(a)–2(c), respectively. By estimation with the 1-D hydrodynamic code "HIMICO"[19,20] for the three cases: the timings of the ablating foam layers, when the density of the boundary between plastic and foam layer becomes the critical density n_{cr}, are +320, +320, and +430 ps, respectively. Since the formation of the plasma shoulder should have a slight time delay compared with the ablation timing, the timing of the SSRT for each target is certainly consistent with the ablation timing.

Actual plasma shoulder formation has not been reproduced by the 1-D simulation because of the difficulties of modeling nonuniform ablation due to the foam structure and the laser speckles. The more detailed analysis of this process should be discussed separately.

V. SUMMARY

We measured time-resolved SRS spectra from spherical plasmas irradiated with 527 nm irradiated random phased laser light. When the two-layered spherical (TLS) targets with a 1 μm thick outer-plastic layer were irradiated with 12 beams, the spectrally shifted Raman light with time (SSRT) were observed for the first time. The very close similarities of the SSRT [Figs. 2(a)–2(c)] between the TLS and the thin foil [Fig. 2(e)] experiments, and the theoretical prediction[16] lead us to interpret that the plasma shoulder exists on the expanding plasma. The SSRT could be excited on the plasma shoulder, whose spectral shift is due to the decrease of the density of the plasma shoulder. The short-wavelength cutoff of the SSRT indicates that the plasma shoulder propagates outward from the TLS target. We estimate the length of the plasma shoulder to be less than 5.7 μm. The timing of the

SSRT is consistent with the one when the inner foam layer is directly ablated by the laser light, predicted by the 1-D hydrodynamic code "HIMICO."[19,20]

Depending on the target parameters such as material and thickness, the SSRT could be excited in a locally perturbed region on an expanding corona plasma. If the SSRT is emitted at an early time of the laser pulse, hot electrons from this instability could cause undesirable preheating of the fuel.

ACKNOWLEDGMENTS

The authors wish to acknowledge the invaluable support by Dr. D. W. Vick and H. Yamamoto, and helpful comments by Dr. S. Kuruma. This experiment could not have been possible without considerable effort of the laser operation by the GOD group, and the target fabrication by the T group.

M. Tsukamoto is financially supported by the Japan Society for the Promotion of Science (JSPS).

[1] W. L. Kruer, *The Physics of Laser Plasma Interactions* (Addison–Wesley, Redwood City, CA, 1987), p. 73.
[2] D. M. Villeneuve, R. L. Keck, B. B. Afeyan, W. Seka, and E. A. Williams, Phys. Fluids **27**, 721 (1984).
[3] K. G. Estabrook, W. L. Kruer, and B. F. Lasinski, Phys. Rev. Lett. **45**, 1399 (1980).
[4] R. P. Drake, R. E. Turner, B. F. Lasinski, K. G. Estabrook, E. M. Campbell, C. L. Wang, D. W. Phillion, E. A. Williams, and W. L. Kruer, Phys. Rev. Lett. **53**, 1739 (1984).
[5] R. P. Drake, R. E. Turner, B. F. Lasinski, E. A. Williams, K. G. Estabrook, W. L. Kruer, E. M. Campbell, and T. W. Johnston, Phys. Rev. A **40**, 3219 (1989).
[6] M. Tsukamoto, R. Kodama, M. Kado, H. Ito, M. Yasumoto, T. Norimatsu, M. Nakai, K. A. Tanaka, T. Yamanaka, and S. Nakai, Rev. Laser Eng. **18**, 724 (1990) (in Japanese).
[7] M. Takagi, T. Norimatsu, T. Yamanaka, S. Nakai, and H. Ito, J. Vac. Sci. Technol. A **9**, 820 (1991).
[8] T. Norimatsu, H. Ito, C. Chen, M. Yasumoto, M. Tsukamoto, K. A. Tanaka, T. Yamanaka, and S. Nakai, Rev. Sci. Instrum. **63**, 3378 (1992).
[9] A. Richard, K. A. Tanaka, K. Nishihara, M. Nakai, M. Katayama, Y. O. Fukuda, T. Kanabe, Y. Kitagawa, T. Norimatsu, T. Yamanaka, M. Kado, T. Kawashima, C. Chen, M. Tsukamoto, and S. Nakai, Phys. Rev. E **49**, 1520 (1994).
[10] R. Kodama, Ph.D. thesis, Osaka University, 1990.
[11] *World Survey of Activities in Controlled Fusion Research*, Nucl. Fusion special supplement 1991 (International Atomic Energy Agency, Vienna, 1991), p. 236.
[12] Y. Kato, K. Mima, N. Miyanaga, S. Arinaga, Y. Kitagawa, M. Nakatsuka, and C. Yamanaka, Phys. Rev. Lett. **53**, 1057 (1984).
[13] R. E. Turner, D. W. Phillion, B. F. Lasinski, and E. M. Campbell, Phys. Fluids **27**, 511 (1984).,
[14] D. M. Villeneuve and H. A. Baldis, Phys. Fluids **31**, 1790 (1988).
[15] C. Labaune, H. A. Baldis, E. Fabre, F. Briand, D. M. Villeneuve, and K. Estabrook, Phys. Fluids B **2**, 166 (1990).
[16] S. Miyamoto, M. Eng. thesis, Osaka University, 1994 (in Japanese).
[17] See Ref. 1, p. 80.
[18] R. P. Drake, E. A. Williams, P. E. Young, K. Estabrook, W. L. Kruer, D. S. Montgomery, H. A. Baldis, and T. W. Johnston, Phys. Fluids B **1**, 2217 (1989).
[19] See Ref. 11, p. 365.
[20] T. Yabe and C. Yamanaka, Comments Plasma Phys. Controlled Fusion **9**, 169 (1985).